

Extension of the “1201” Family to Strontium-Rich Chromite and Ferrite, $\text{Bi}_{0.4}\text{Sr}_{2.5}\text{Cr}_{1.1}\text{O}_{4.9}$ and $\text{Bi}_{0.4}\text{Sr}_{2.5}\text{Fe}_{1.1}\text{O}_5$

M. Allix, D. Pelloquin,¹ F. Studer, N. Nguyen, A. Wahl, A. Maignan, and B. Raveau

Laboratoire de Cristallographie et Sciences des Matériaux, UMR 6508-CNRS, ISMRA et Université de Caen 6, Boulevard du Maréchal Juin, 14050 CAEN Cedex, France

Received February 15, 2002; accepted April 12, 2002

Two new Sr-rich “1201”-type oxides, $\text{Bi}_{0.4}\text{Sr}_{2.5}\text{Cr}_{1.1}\text{O}_{4.9}$ and $\text{Bi}_{0.4}\text{Sr}_{2.5}\text{Fe}_{1.1}\text{O}_5$ have been synthesized. These compounds, intergrowths of double rock-salt layers with single perovskite layers, show a 1:1 ordering between (Bi,*M*) and Sr species within the intermediate rock-salt layer [$\text{Bi}_{0.4}\text{M}_{0.1}\text{Sr}_{0.5}\text{O}$]. The XANES study shows that bismuth is mainly trivalent, whereas iron is mixed valent containing 50% Fe^{3+} and 50% Fe^{4+} (also confirmed by Mössbauer), and chromium could be a mixture of Cr^{3+} and Cr^{6+} sitting in the perovskite and rock-salt-type sites, respectively. Both compounds exhibit antiferromagnetic interactions. The Cr-phase is a strong insulator, whereas the Fe-phase exhibits a semi-conductor-like resistivity whose value at room temperature is close to that of isotypic cobaltite. © 2002

Elsevier Science (USA)

Key Words: layered oxides; Xanes and Mössbauer spectroscopies; TEM analyses.

INTRODUCTION

After the discovery of superconductivity in the “2201”-type structure of $\text{Bi}_2\text{Sr}_2\text{CuO}_6$ (1), trivalent bismuth has been considered as a potential element for the stabilization of layered structures leading to closely related cuprates $\text{Bi}_2\text{A}_{n+1}\text{Cu}_n\text{O}_{2n+4}$ (2, 3) with higher T_c , and to isotypic cobaltite, manganite and ferrite with the 2201 structure (4–8). Recent investigations of the systems Bi–Sr–*M*–O with *M* = Mn and Co, have shown the important role of bismuth for the synthesis of new strontium-rich “1201”-type oxides $\text{Bi}_{0.4}\text{Sr}_{2.5}\text{M}_{1.1}\text{O}_{5-\delta}$ (8, 9). Like the classical “1201” structure, these compounds exhibit single perovskite layers intergrown with double rock-salt (RS) layers. However, they differ from the latter by the nature of the RS layers, which are formed of an intermediate slab containing mainly Bi^{3+} and Sr^{2+} and some additional cobalt or manganese, sandwiched between two strontium

slabs. It is indeed observed that intermediate RS slab exhibits a 1:1 ordering of the (Bi,*M*) and Sr atoms.

In contrast to copper, cobalt and manganese, ferrites and chromites do not show any Bi-2201 or Bi-1201 structures although $\text{Bi}_2\text{Sr}_3\text{Fe}_2\text{O}_9$, 2212-type ferrite was synthesized (10), isotypic to the corresponding manganite (11). In order to enlarge the chemistry of these layered compounds, we have explored the systems Bi–Sr–Fe–O and Bi–Sr–Cr–O. We describe herein the synthesis, crystal structure, and magnetotransport properties of two new Sr-rich 1201 oxides, $\text{Bi}_{0.4}\text{Sr}_{2.5}\text{Fe}_{1.1}\text{O}_5$ and $\text{Bi}_{0.4}\text{Sr}_{2.5}\text{Cr}_{1.1}\text{O}_{4.9}$, characterized again by 1:1 ordering between bismuth and strontium in the intermediate RS layer. We also show the existence of continuous solid solutions between the pure iron 1201-phase and other 1201 oxides (*M* = Mn, Cr, and Co).

CHEMICAL SYNTHESSES

In a first step, the investigations of the 1201 phases in the Bi–Sr–Fe–O and Bi–Sr–Cr–O systems were performed on the basis of the nominal compositions $\text{Bi}_{0.5\pm x}\text{Sr}_{2.5\pm x'}\text{M}_{1\pm x''}\text{O}_{5-\delta}$ (*M* = Cr, Fe), varying *x*, *x'*, and *x''* from 0 to 0.2 and controlling δ through the SrO/SrO₂ ratio. In a second step, syntheses were carried out with nominal compositions corresponding to the average cation content obtained from EDS analyses. The same method was used to study the solubility range $\text{Bi}_{0.5-x}\text{Sr}_{2.5-x'}\text{Fe}_{1.1-y}\text{M}_y\text{O}_{5-\delta}$ (*M* = Cr, Mn, Co).

Each sample was prepared in a dry box, starting from the appropriate mixture of oxides Bi_2O_3 , M_2O_3 (*M* = Fe, Mn, Cr), Co_3O_4 , SrO and SrO₂. The presence of carbon dioxide or carbonate groups must absolutely be avoided, since it may indeed lead to the formation of oxycarbonates as recently reported in the Sr–Fe–O system (12, 13). To avoid the carbonate contamination, SrO was freshly prepared by heating SrO₂ or $\text{Sr}(\text{OH})_2 \cdot 8\text{H}_2\text{O}$ at 1100°C. The mixtures, intimately ground in an agate mortar, were placed in an evacuated quartz ampoule and heated up to a

¹To whom correspondence should be addressed. Fax: 02-31-96-16-00. E-mail: pelloquin@ismra.fr.

temperature close to 1000°C at 15°C h⁻¹, kept at this temperature for 24 h and quenched to room temperature.

EXPERIMENTAL TECHNIQUES

The electron diffraction (ED) studies were carried out using a JEOL 200CX microscope fitted with an eucentric goniometer ($\pm 60^\circ$) while the high-resolution electron microscopy (HREM) images and convergent beam electron diffraction (CBED) pattern were recorded with a TOPCON 002B microscope operating at 200 kV and having a point resolution of 1.8 Å. Energy dispersive spectroscopy (EDS) analyses were systematically carried out, both electron microscopes being equipped with KEVEX analyzers.

Oxygen content was determined by chemical analysis using redox titration.

The X-ray powder diffraction (XRPD) data were collected at room temperature with two vertical diffractometers: a Philips X'PERT PRO and a Philips PW 1830. Both diffractometers are working with CuK α radiation. Data were collected by step scanning over an angular range $10^\circ \leq 2\theta \leq 120^\circ$ by increments of 0.02° (2θ) and were treated by profile analysis with the program Fullprof (14).

Magnetic susceptibility $\chi(T)$ measurements were investigated at low temperature (5–400 K) using an AC–DC SQUID Quantum Design magnetometer and at high temperature (300–700 K) using the Faraday method with, in both cases, an applied field of 3 kG. Resistivity measurements were recorded with a physical properties measurements system (PPMS) from Quantum Design (four-probe method).

The ⁵⁷Fe Mössbauer spectrum at room temperature of the powdered Bi_{0.4}Sr_{2.5}Fe_{1.1}O₅ sample was recorded using a conventional spectrometer operating in the constant acceleration mode. ⁵⁷Co/Rh was used as the γ -ray source. The isomer shift (IS) is referred to metallic iron.

The X-ray absorption spectra at Fe K-, Cr K- and Bi L₃-edge were recorded at room temperature in a classical transmission mode at the EXAFS I station (channel cut monochromator) using the synchrotron radiation of the DCI storage ring of LURE (Orsay, France). The energy resolution at the Fe and the Cr K-edge is estimated to be 1.3 eV and at Bi L₃-edge to 5.9 eV whereas the reproducibility of the monochromator position is as high as 0.3 eV. An iron metal K-edge, chromium metal K-edge or bismuth metal L₃-edge was run simultaneously for precise energy calibration. The relative energies between various spectra were established by a careful comparison of the derivative metal transition spectra. The normalization procedure used through this work was a standard one: after subtraction of the same diffusion background on the XANES and EXAFS spectra, recorded in the same experimental

conditions, a point located at an energy of 800 eV from the edge, where no more EXAFS oscillations were still observable, was set to unity. Then the intensity of a point with an energy between 50 and 100 eV from the edge was recorded on the EXAFS spectrum and reported on the normalized height.

RESULTS AND DISCUSSION

Under the experimental conditions, the study of the system with closing nominal compositions Bi_{0.4}Sr_{2.5}FeO₅ and Bi_{2/3}Sr_{2.5}CrO₅ has allowed to stabilize nearly pure samples. During the synthesis of chromium-based sample, the formation of bismuth metal as droplets could not be avoided. The corresponding XRPD patterns (Fig. 1) show that they are closely related to the tetragonal 1201-type structure observed for Tl_{0.5}Pb_{0.5}Sr₂CuO₅ (15) and (Bi_{0.4}Sr_{0.45}Co_{0.15})Sr₂CoO_{4.85} (9). In a second step, the solubility range Fe_{1.1-y}M_y has been scanned substituting cobalt, manganese, and chromium for iron in order to study possible magnetic interactions.

The EDS analyses carried out on numerous microcrystals of each sample lead to the same average cationic composition, namely Bi_{0.4}Sr_{2.5}Fe_{1.1} and Bi_{0.4}Sr_{2.5}Cr_{1.1}. This suggests that the structure of these compounds is close to that previously reported for the cobaltite Bi_{0.4}Sr_{2.45}Co_{0.15}O_{5- δ} (9), i.e., the excess of transition element with regard to the theoretical 1201 formula is located in the mixed (Bi,Sr)O plane leading to the actual formula (Bi_{0.4}M_{0.1}Sr_{0.5})Sr₂MO_{5- δ} . On this basis, the chemical analyses lead to an actual oxygen deficiency δ close to 0 for M = Fe and to 0.1 for M = Cr.

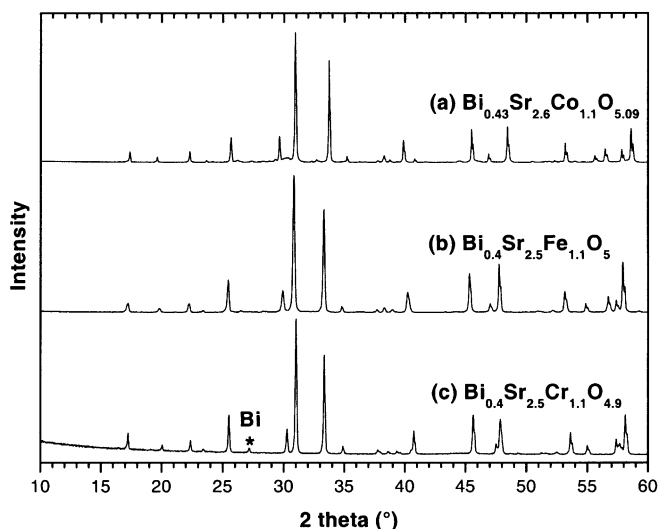


FIG. 1. Experimental X-ray diffraction patterns for the 1201-ferrite: Bi_{0.4}Sr_{2.5}Fe_{1.1}O₅ (b) and the 1201-chromite: Bi_{0.4}Sr_{2.5}Cr_{1.1}O_{4.9} (c) in comparison with the tetragonal 1201-cobaltite: Bi_{0.4}Sr_{2.45}Co_{0.15}O_{4.85} (a).

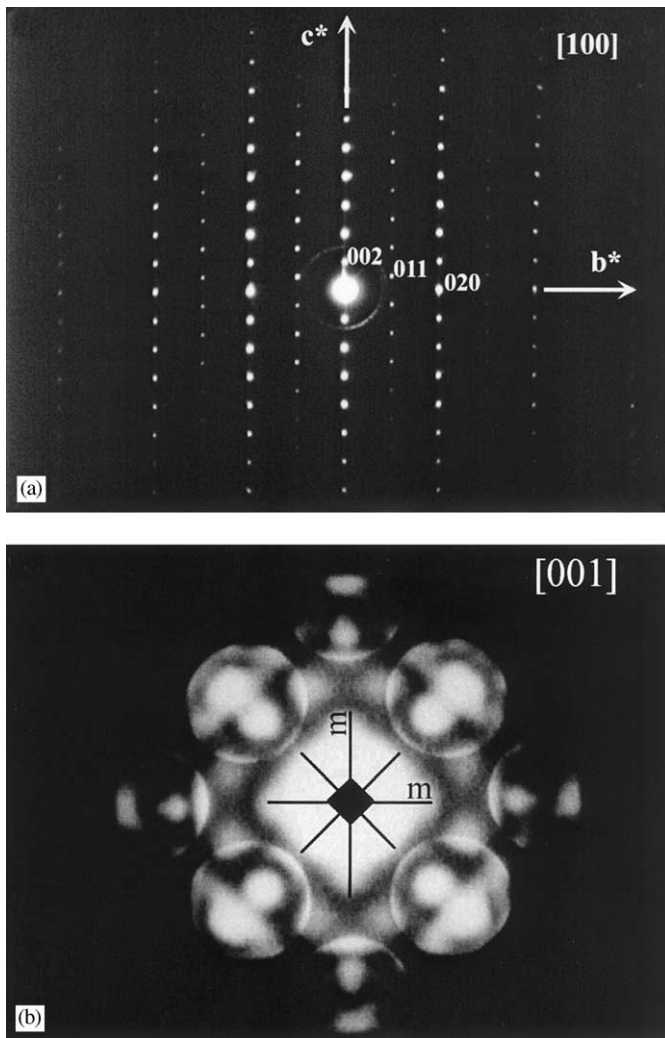


FIG. 2. Experimental ED [100] oriented pattern (a) and CBED [001] oriented pattern (b) indexed in the $(a_p\sqrt{2} \times a_p\sqrt{2} \times 2c_{1201})$ lattice.

Structural Investigations

The reciprocal space was reconstructed for characteristic crystallites from ED patterns by tilting around the crystallographic axes. The analysis shows that these two new phases are related to a perovskite-layered structure. The system of reflections evidences a tetragonal cell with $a = b \approx a_p \sqrt{2}$ (a_p is the parameter of the cubic perovskite-type structure) and $c = 2c_{1201} \approx 18 \text{ \AA}$ while the main condition limiting the reflections, $hkl: h+k+l=2n$ implies a *I*-type lattice. The characteristic ED [100] oriented pattern is shown in Fig. 2a.

This tetragonal symmetry is confirmed by the complementary convergent beam electron diffraction (CBED) study carried out on the [001] oriented patterns (Fig. 2b). The analysis of direct beam (bright field mode) shows clearly two perpendicular *m* mirrors and evidences the four-fold axis existence. These symmetry elements are also

observed for the whole pattern. Thus, the tetragonal *I4/mmm* space group can be proposed. Consequently, the refinements of XRPD patterns of both phases, indexed in this tetragonal cell, lead to the following parameters:

$$a = 5.3833(1) \text{ \AA} \quad \text{and} \quad c = 17.9639(2) \text{ \AA} \quad \text{for } M = \text{Fe}$$

and

$$a = 5.3696(1) \text{ \AA} \quad \text{and} \quad c = 17.6970(3) \text{ \AA} \quad \text{for } M = \text{Cr}.$$

In order to confirm the layer stacking mode of these new iron- and chromium-based oxides and to determine the origin of the superstructure, especially the doubling of the c_{1201} parameter, an HREM study was performed. Typical images, recorded in the case of $\text{Bi}_{0.4}\text{Sr}_{2.5}\text{Cr}_{1.1}\text{O}_{4.9}$, are given in Fig. 3, where high electron density zones are highlighted. The best orientation to image the layer stacking is the $[100]_p$, i.e., the $[110]$ orientation in the supercell. At the edge of the crystal, the contrast consists of three adjacent rows

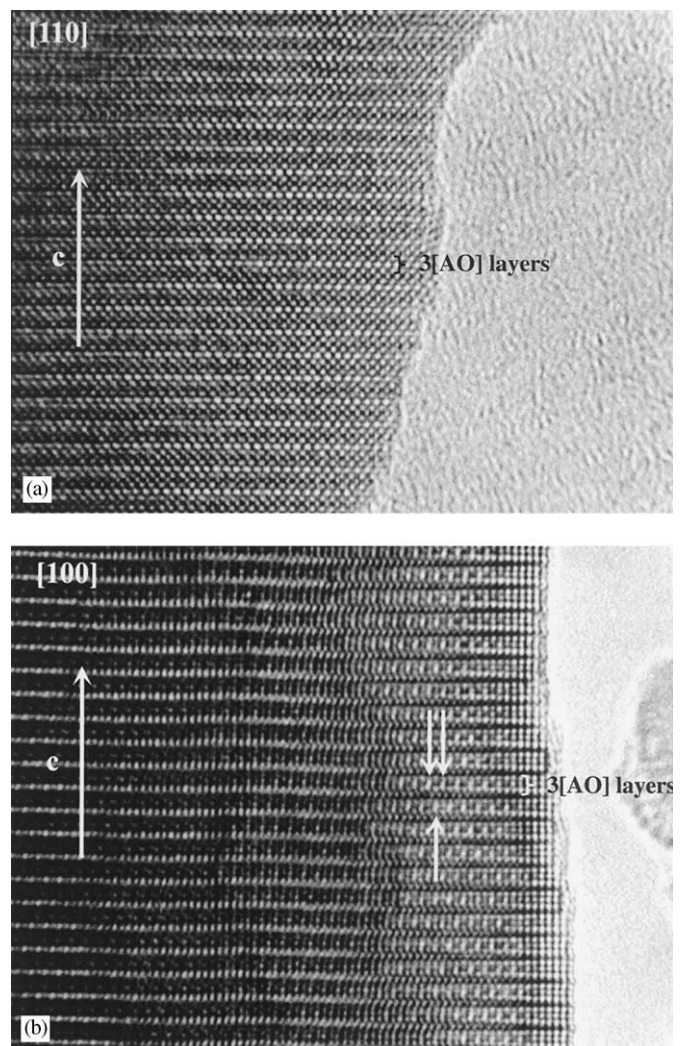


FIG. 3. Experimental HREM image recorded along the [110] (a) and the [100] (b) directions. Bright dots are correlated to Bi and Sr positions.

of bright dots separated by a single row of smaller bright dots (Fig. 3a). They are, respectively, correlated to triple [AO] layers and a single [CrO_{2-δ}] layer, in agreement with a 1201-type stacking mode. Here again, the cationic composition suggests the formation of one mixed Bi/Sr layer. The actual information about the superstructure is given by the [100] oriented crystals. This point is shown in Fig. 3b. At the level of the single mixed layer sandwiched between two [SrO]_∞ layers, the alternation of one bright dot with one less bright dot is observed, leading to a periodicity of 5.4 Å. This contrast is shifted by $a_p\sqrt{2}/2$ in the adjacent RS block (see white arrows in Fig. 3b), explaining the doubling of the c_{1201} parameter. Taking into account the actual (Bi+Cr)/Sr ratio determined by the EDS analyses and previous HREM observations reported in the Bi–Sr–M–O system (6–10), such a contrast can be interpreted as the formation of mixed Bi/Cr/Sr layers, especially by a 1:1 ordering between (Bi,Cr) and Sr species within the intermediate RS layer, leading to alternating files of (Bi,Cr) and Sr atoms, running along the [100] direction. Each ordered layer is sandwiched between two [SrO] layers along \vec{c} according to the [SrO][(Bi,Cr)_{0.5}Sr_{0.5}O][SrO] sequence. This structural feature leads to the doubling of the c_{1201} -axis in agreement with the *I* symmetry. Note that this ordering at the level of the intermediate [AO] layer has been also reported in Bi_{0.4}Sr_{2.45}Co_{1.15}O_{5-δ} (9)1201-type phases while the quadrupling of the c_{1201} is observed in the case of Bi_{0.4}Sr_{2.6}MnO_{4.7} (8).

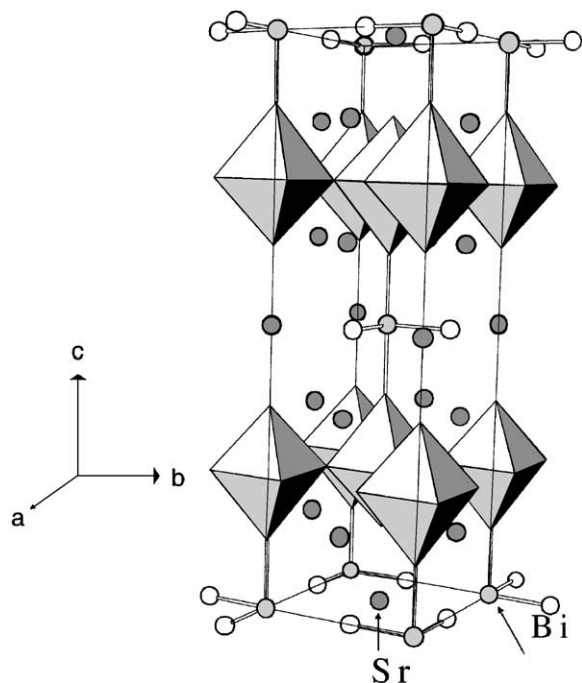


FIG. 4. Perspective view of the Bi_{0.4}Sr_{2.5}Fe_{1.1}O₅ ferrite and the Bi_{0.4}Sr_{2.5}Cr_{1.1}O_{4.9} chromite.

In order to check this structural model (Fig. 4), structural refinements were carried out from XRPD data in the *I4/mmm* space group. Taking into account the partial occupancy of the Bi site by Fe or Cr atoms and fixing B factors for oxygens, we obtain the final agreement factors: $R_{\text{Bragg}} = 0.077$ and $\chi^2 = 2.96$ for iron-based 1201-type structure and $R_{\text{Bragg}} = 0.069$ and $\chi^2 = 2.51$ for chromium-based 1201-type structure, respectively. These results confirm that these new layered oxides exhibit the 1201-type structure with a Bi–Sr ordering and a partial substitution of Bi by Fe or Cr in the intermediate layer [Bi_{0.4}M_{0.1}Sr_{0.5}O] in good agreement with EDS results. The final refined parameters are given in Table 1 while the main interatomic distances (Table 2) show a highly distorted octahedral environment for iron or chromium atoms in the transition metal–oxygen planes with four short equatorial distances ($M\text{--}O(4)$), one medium ($M\text{--}O(3)$) and one long ($M\text{--}O(2)$) apical bond distance. From these refinements, the oxygen vacancies seem to be located at the level of the intermediate mixed [(Bi,Cr)_{0.5}Sr_{0.5}O] RS layer. Nevertheless, an accurate study of the structure by neutron diffraction will be necessary to clarify the oxygen content and positions in Bi_{0.4}Sr_{2.5}Cr_{1.1}O_{4.9}.

In the same way, the partial substitutions of cobalt, manganese, and chromium for iron have been analyzed. The cell parameters evolution versus the composition of the mixed Fe_{1.1-y}M_y 1201 is shown in Fig. 5, while the corresponding EDS analyses and main structural parameters are listed in Table 3. The non-linear curves (Fe/Co and Fe/Mn) are explained by the oxygen stoichiometry, ranging from “O₅” to “O_{4.8}” for cobalt and being equal to “O_{4.7}” for Mn. Among these results, a perfect range of solubility between iron and manganese, cobalt and chromium, respectively, is observed. No specific ordering has been detected at room temperature between the transition elements whatever the Fe/*M* ratio.

XANES Study

In order to obtain more information about the main formal charge and the environment of bismuth, chromium, and iron species in Bi_{0.4}Sr_{2.5}Fe_{1.1}O₅ and Bi_{0.4}Sr_{2.5}Cr_{1.1}O_{4.9}, XANES investigations were carried out.

Bismuth L₃-Edge Study

XANES spectra at Bi L₃-edge for the reference compounds (Bi₂O₃ for Bi³⁺ and NaBiO₃ for Bi⁵⁺) and for the 1201-type ferrite and chromite (the same curve has been registered for both of them) are presented in Fig. 6. The environments are regular octahedra with a single Bi–O distance in NaBiO₃ (16) and two types of distorted octahedral coordination in Bi₂O₃ (17). As expected, an energy shift between the two reference compounds can be

TABLE 1
Refined Structural Parameters for $\text{Bi}_{0.4}\text{Sr}_{2.5}\text{Fe}_{1.1}\text{O}_5$ and $\text{Bi}_{0.4}\text{Sr}_{2.5}\text{Cr}_{1.1}\text{O}_{4.9}$

Atom	Site	x	y	z	B (\AA^2)	n
1201 Fe						
Bi/Fe	2a	0.0	0.0	0.0	1.0(1)	1.58(2)/0.42(2)
Sr(1)	2b	0.0	0.0	0.5	0.2(1)	2
Sr(2)	8g	0.5	0.0	0.1481(1)	0.3(1)	8
Fe	4e	0.0	0.0	0.2500	0.1(1)	4
O(1)	8i	0.400(4)	0.0	0.0	1.0 ^a	4
O(2)	4e	0.0	0.0	0.124(1)	1.0 ^a	4
O(3)	4e	0.5	0.5	0.133(1)	1.0 ^a	4
O(4)	8f	0.25	0.25	0.25	1.0 ^a	8
1201Cr						
Bi/Cr	2a	0.0	0.0	0.0	0.35(4)	1.8(1)/0.2(1)
Sr(1)	2b	0.0	0.0	0.5	0.0(1)	2
Sr(2)	8g	0.5	0.0	0.1490(1)	0.0(1)	8
Cr	4e	0.0	0.0	0.2500	0.0(1)	4
O(1)	8i	0.423(4)	0.0	0.0	0.3(2)	3.8(1)
O(2)	4e	0.0	0.0	0.133(1)	0.3(2)	4
O(3)	4e	0.5	0.5	0.131(1)	0.3(2)	4
O(4)	8f	0.25	0.25	0.25	0.3(2)	8

^aParameter not refined.

seen, in connection with bismuth formal charge. The A shoulder in the NaBiO_3 spectra can be assigned to the specific transition $2p_{3/2} \rightarrow 6s$ (18) which can only be seen in the case of Bi^{5+} because $6s$ orbitals are assumed to be empty. Considering now the Bi L_3 -edge of our 1201 phase, it appears that the measured energy of the main jump midheight (EMJM = 6.2 eV) can be compared to the Bi^{3+} reference (EMJM = 5.9 eV) and well separated from the Bi^{5+} reference (EMJM = 8.6 eV) as seen in Table 4. It indicates that the bismuth formal charge is nearly equal to +3. But, considering the not-well-defined A shoulder, due to the signal-to-noise ratio induced by the small amount of Bi in the 1201-type structure, we cannot exclude the presence of mixed formal charge $\text{Bi}^{3+}/\text{Bi}^{5+}$ with small quantities of Bi^{5+} . Moreover, Rao and Wang (18) have

shown that B and C peaks can be assigned to the specific transitions $2p_{3/2} \rightarrow 6d(t_{2g})$ and $2p_{3/2} \rightarrow 6d(e_g)$, respectively, due to the splitting of the $6d$ states into non-bonding orbitals (t_{2g}) and antibonding orbital (e_g). These peaks are well separated in the two phases because of a better concentration of Bi–O distances compared to the one present in Bi_2O_3 .

Iron K-Edge Study

Figure 7a shows the spectra at Fe K-edge registered for the 1201 ferrite and three references: Fe_2O_3 for Fe^{3+} which exhibits a distorted octahedral coordination (19), SrFeO_{3-x} ($x \approx 0.15$) representing a mixed $\text{Fe}^{3+}/\text{Fe}^{4+}$ reference involving another distorted octahedral coordination (20) and $\text{Sr}_2\text{FeCoO}_6$ (21) for the Fe^{4+} reference. In a first step, the measured energy of the midheight of the main peak of our 1201-ferrite (Table 4) compared with those obtained for Fe_2O_3 , SrFeO_{3-x} , $\text{Sr}_2\text{FeCoO}_6$ suggests a mixed $\text{Fe}^{3+}/\text{Fe}^{4+}$ formal charge with equal amount of Fe^{3+} and Fe^{4+} . From the edge value of our ferrite given in Table 4, an equivalent amount of Fe^{3+} and Fe^{4+} species can be deduced. Nevertheless, a first pre-edge A can be observed. It is due to a hybridization of $\text{Fe}(4p)\text{--O}(2p)\text{--Fe}(3d)$ orbitals. This hybridization is stronger for non-centrosymmetric environment like tetrahedral environment compared to octahedral environment (22), and allows partly the forbidden $1s \rightarrow 3d$ transition to be visible (23). Considering our structure, a tetrahedral environment can be excluded from the small-intensity pre-edge A which is comparable to the one of the other references, in agreement with the structural results.

TABLE 2
Main Interatomic Distances in $\text{Bi}_{0.4}\text{Sr}_{2.5}\text{Fe}_{1.1}\text{O}_5$ and $\text{Bi}_{0.4}\text{Sr}_{2.5}\text{Cr}_{1.1}\text{O}_{4.9}$

$M\text{--O}$	Distance (\AA)	Distance (\AA)	n
	1201-Fe	1201-Cr	
Bi/ $M\text{--O}$ (1)	2.16(2)	2.27(2)	$\times 4$
Bi/ $M\text{--O}$ (2)	2.23(2)	2.35(2)	$\times 2$
Sr(1) --O (1)	2.745(4)	2.72(1)	$\times 8$
Sr(1) --O (3)	2.39(2)	2.32(2)	$\times 2$
Sr(2) --O (1)	2.714(4)	2.67(1)	$\times 2$
Sr(2) --O (2)	2.726(3)	2.70(1)	$\times 2$
Sr(2) --O (3)	2.705(2)	2.70(2)	$\times 2$
Sr(2) --O (4)	2.641(1)	2.61(0)	$\times 4$
$M\text{--O}$ (2)	2.39(2)	2.08(2)	$\times 1$
$M\text{--O}$ (3)	1.97(2)	2.11(2)	$\times 1$
$M\text{--O}$ (4)	1.908(1)	1.898(1)	$\times 4$

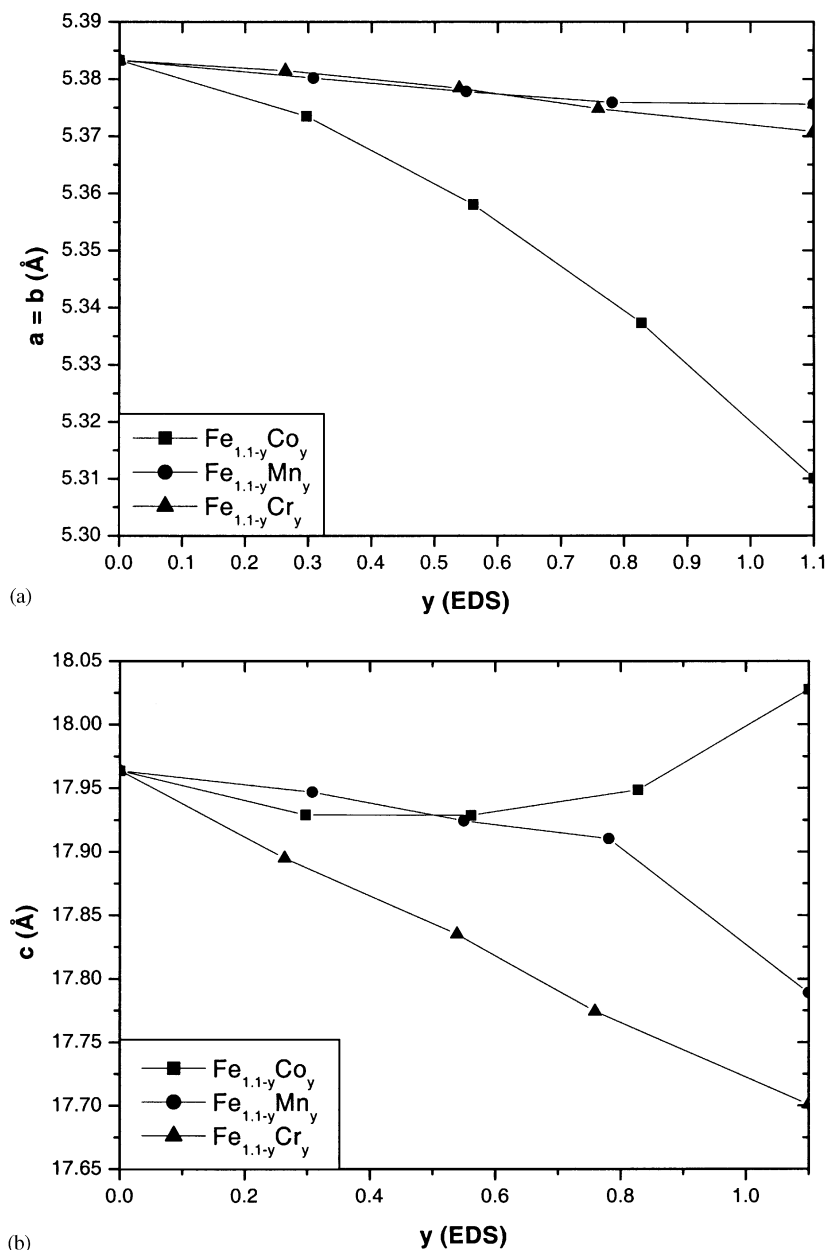


FIG. 5. Evolution of parameters in the system: $\text{Bi}_{0.4}\text{Sr}_{2.5}\text{Fe}_{1.1-y}\text{O}_{5-\delta}$.

Natoli and co-workers (24) have shown that the peak energies on a XANES spectra can be linked empirically to the $M\text{-O}$ distance through the simple relationship: $(E - E_0) \times R^2 = K$ which holds for transition metal compounds and high-energy transitions. E is corresponding to the peak energy and R to the $M\text{-O}$ distance, whereas E_0 and K are constants determined for a given edge and environment. To apply the so-called Natoli's rule to the Fe K-edge, one needs to determine E_0 and K constants through a precise knowledge of the Fe-O distances in the reference oxides Fe_2O_3 (19) and $\text{SrFeO}_{2.85}$ (20) as shown in Table 4. The Fe-O distances (noted B and C in Fig. 7a)

corresponding to the ferrite are calculated as 2.2 \AA (B) and 1.92 \AA (C), respectively. These values are in agreement with XRPD results with four short equatorial distances at 1.908 \AA and two longer apical distances (1.97 and 2.39 \AA). Peaks B and C correspond to $1s \rightarrow 4p$ transitions in the $3d^5 \underline{L}$ configuration for non-bonding (long distances) and antibonding (short distances levels).

Chromium K-Edge Study

The chromium K-edge of $\text{Bi}_{0.4}\text{Sr}_{2.5}\text{Cr}_{1.1}\text{O}_{4.9}$ and of the three reference oxides, NdCrO_3 for Cr^{3+} , CrO_2 for Cr^{4+}

TABLE 3
EDS Results and Main Structural Parameters for the Series $\text{Bi}_{0.4}\text{Sr}_{2.5}\text{Fe}_{1.1-y}\text{O}_{5-\delta}$ ($M = \text{Co}, \text{Mn}, \text{and Cr}$)

EDS composition	a (Å)	c (Å)
$\text{Bi}_{0.4}\text{Sr}_{2.5}\text{Fe}_{1.1}\text{O}_5$	5.3833(1)	17.964(0)
$\text{Bi}_{0.4}\text{Sr}_{2.5}\text{Fe}_{0.8}\text{Cr}_{0.3}\text{O}_{5-\delta}$	5.3815(6)	17.895(1)
$\text{Bi}_{0.4}\text{Sr}_{2.5}\text{Fe}_{0.55}\text{Cr}_{0.55}\text{O}_{5-\delta}$	5.3784(3)	17.835(3)
$\text{Bi}_{0.4}\text{Sr}_{2.5}\text{Fe}_{0.24}\text{Cr}_{0.76}\text{O}_{5-\delta}$	5.3748(1)	17.774(0)
$\text{Bi}_{0.4}\text{Sr}_{2.5}\text{Cr}_{1.1}\text{O}_{4.9}$	5.3696(1)	17.6979(3)
$\text{Bi}_{0.4}\text{Sr}_{2.5}\text{Fe}_{0.8}\text{Co}_{0.3}\text{O}_{5-\delta}$	5.3735(4)	17.929(6)
$\text{Bi}_{0.4}\text{Sr}_{2.5}\text{Fe}_{0.54}\text{Co}_{0.56}\text{O}_{5-\delta}$	5.3581(2)	17.929(5)
$\text{Bi}_{0.4}\text{Sr}_{2.5}\text{Fe}_{0.27}\text{Co}_{0.83}\text{O}_{5-\delta}$	5.3373(3)	17.949(5)
$\text{Bi}_{0.4}\text{Sr}_{2.5}\text{Fe}_{0.79}\text{Mn}_{0.31}\text{O}_{5-\delta}$	5.3802(4)	17.947(7)
$\text{Bi}_{0.4}\text{Sr}_{2.5}\text{Fe}_{0.54}\text{Mn}_{0.56}\text{O}_{5-\delta}$	5.3778(6)	17.924(1)
$\text{Bi}_{0.4}\text{Sr}_{2.5}\text{Fe}_{0.32}\text{Mn}_{0.78}\text{O}_{5-\delta}$	5.3759(8)	17.910(4)

and $\text{K}_2\text{Cr}_2\text{O}_7$ for Cr^{6+} formal charges, are shown in Fig. 7b. The energy of main jump midheight (Table 4) allows the oxidation state of chromium in $\text{Bi}_{0.4}\text{Sr}_{2.5}\text{Cr}_{1.1}\text{O}_{4.9}$ to be fixed at a higher value than Cr^{3+} , namely close to +3.4. From this result, mixed valence states between Cr^{3+} and Cr^{4+} or Cr^{3+} and Cr^{6+} can be proposed for chromium species. In fact, as it has been already seen in $\text{Hg}_{0.5}\text{Cr}_{0.5}\text{Sr}_2\text{CuO}_{4.82}$ (23), the Cr part substituted to Bi ions might be hexavalent and the Cr species in the $[\text{CrO}_2]$ layers could be trivalent (for instance, 10% of Cr^{6+} leads to a +3.3 formal charge). Moreover, the intensity of the pre-peak is in agreement with a distorted octahedral environment of chromium. The differences between NdCrO_3 , $\text{Bi}_{0.4}\text{Sr}_{2.5}\text{Cr}_{1.1}\text{O}_{4.9}$ and $\text{K}_2\text{Cr}_2\text{O}_7$ arise from the distortion of the oxygen polyhedra around chromium cation. The regular octahedron in NdCrO_3 with six similar Cr–O distances ((Cr–O)

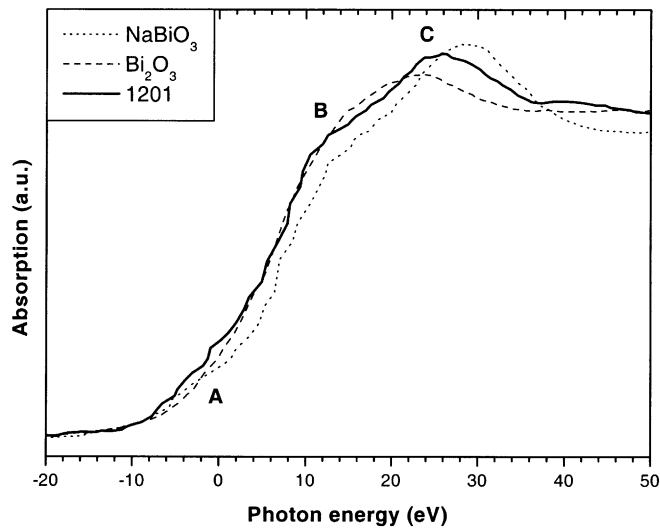


FIG. 6. Bismuth L_3 edges for Bi_2O_3 , NaBiO_3 , the chromite and the ferrite.

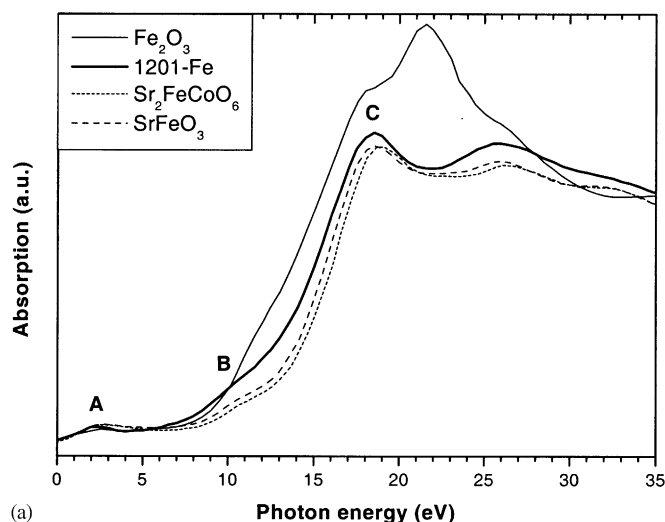
TABLE 4
Formal Charge (FC), d_{M-O} , and EMJM at Bi L_3 -edge, Fe K-edge and Cr K-edge for references, $\text{Bi}_{0.4}\text{Sr}_{2.5}\text{Fe}_{1.1}\text{O}_5$ and $\text{Bi}_{0.4}\text{Sr}_{2.5}\text{Cr}_{1.1}\text{O}_{4.9}$

Compounds	FC	EMJM (eV) ± 0.3 eV	d_{M-O}
Fe_2O_3	+3	13.7	1.94×3 2.11×3
$\text{SrFeO}_{2.85}$	+3.7	15.1	1.92×4 1.98×2
$\text{Sr}_2\text{FeCoO}_6$	+4	15.6	1.92×6
$\text{Bi}_{0.4}\text{Sr}_{2.5}\text{Fe}_{1.1}\text{O}_{5.0}$	+3.4	14.5	1.91×4 1.97×1 2.39×1
NdCrO_3	+3	14.0	1.97×4 1.98×2
CrO_2	+4	16.9	1.78×4 2.08×2
$\text{K}_2\text{Cr}_2\text{O}_7$	+6	18.3 in tetrahedral configuration	$1.54\text{--}1.71$ (Cr(1)) $1.55\text{--}1.86$ (Cr(2)) $1.59\text{--}1.84$ (Cr(3)) $1.51\text{--}1.75$ (Cr(4))
$\text{Bi}_{0.4}\text{Sr}_{2.5}\text{Cr}_{1.1}\text{O}_{4.9}$	+3.4	15.2	1.90×4 2.08×1 2.11×1
NaBiO_3	+5	8.6	
Bi_2O_3	+3	5.9	
$\text{Bi}_{0.4}\text{Sr}_{2.5}\text{Fe}_{1.1}\text{O}_{5.0}$	+3	6.2	

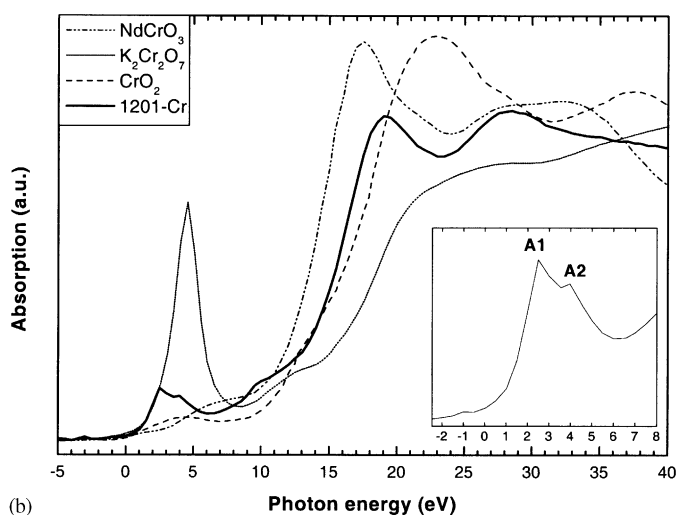
≈ 1.98 Å) generates a strong white line at 17.6 eV due to the occurrence of electronic transitions $1s \rightarrow 4p_{x,y,z}$ at the same energy. Conversely, the octahedral distortion in $\text{Bi}_{0.4}\text{Sr}_{2.5}\text{Cr}_{1.1}\text{O}_{4.9}$ with three sets of Cr–O distances (1.90, 2.08, and 2.10 Å) induces a wide spread of the $1s \rightarrow 4p$ transitions along the x -, y - and z -axis, respectively. By applying Natoli's rule, we have found two distances equal to 1.91 and 2.2 Å, which is in good agreement with the distances calculated from X-ray diffraction. The pre-peak of $\text{Bi}_{0.4}\text{Sr}_{2.5}\text{Cr}_{1.1}\text{O}_{4.9}$ (due to hybridization of $\text{Cr}(3d)\text{--O}(2p)\text{--Cr}(4p)$ orbitals) is observed (inset of Fig. 7b) with a fine structure of two peaks A1 and A2 (2.48 and 3.96 eV), due to the crystal field effect on the Cr $3d$ orbitals: t_{2g} and e_g (separated by a gap of 1.48 eV) in agreement with the distortion of the octahedron.

Mössbauer Study

The spectrum of $\text{Bi}_{0.4}\text{Sr}_{2.5}\text{Fe}_{1.1}\text{O}_5$ compound recorded at room temperature is shown in Fig. 8. It consists of a quadrupolar doublet characterizing pure electric interactions, composed of two broad lines exhibiting an asymmetry. This reveals the existence of different paramagnetic Fe ions. The spectrum is well fitted by accounting for three components with IS and quadrupolar splitting (QS) values given in Table 5. The smallest component noted C



(a)



(b)

FIG. 7. (a) XANES-normalized Fe K-edges at room temperature for iron references and $\text{Bi}_{0.4}\text{Sr}_{2.5}\text{Fe}_{1.1}\text{M}_x\text{O}_5$. (b) XANES-normalized Fe K-edges at room temperature for chromium references and $\text{Bi}_{0.4}\text{Sr}_{2.5}\text{Cr}_{1.1}\text{O}_{4.9}$.

($\text{IS} = 0.13 \text{ mm s}^{-1}$, $\text{QS} = 0.25 \text{ mm s}^{-1}$), with relative intensity about $13 \pm 5\%$, can be attributed to the Fe^{4+} part substituted to Bi ions. Otherwise, the A and B components exhibit two IS values which are significantly different, and correspond indeed, to Fe^{3+} ($\text{IS} = 0.21 \text{ mm s}^{-1}$) and Fe^{4+} ($\text{IS} = 0.08 \text{ mm s}^{-1}$) contribution, respectively, in the iron site. The sum of B and C observed intensities lead to about 50% Fe^{4+} in $\text{Bi}_{0.4}\text{Sr}_{2.5}\text{Fe}_{1.1}\text{O}_5$ compound in agreement with the chemical and XANES analyses.

Physical Properties

$\text{Bi}_{0.4}\text{Sr}_{2.5}\text{Cr}_{1.1}\text{O}_{4.9}$

The temperature dependence of the magnetic susceptibility is shown in Fig. 9a. One observes a strong difference

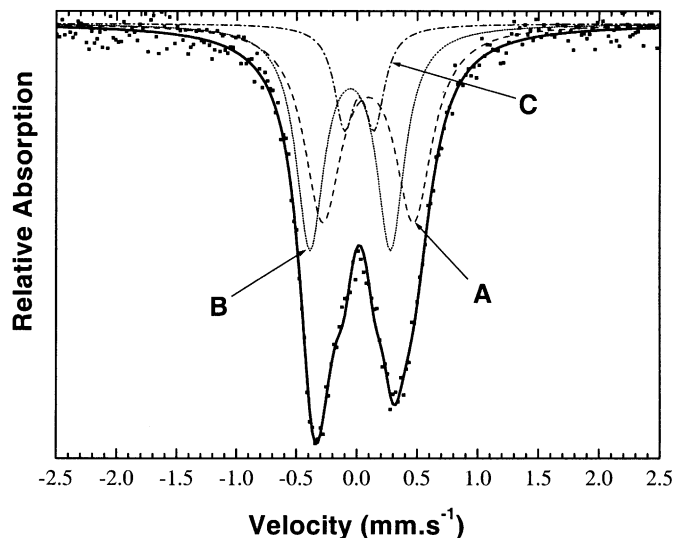


FIG. 8. Mössbauer spectrum of $\text{Bi}_{0.4}\text{Sr}_{2.5}\text{Fe}_{1.1}\text{O}_5$ reported at a room temperature.

between the ZFC and FC mode (3000 G); this pronounced irreversibility is indicative of a magnetic ordering transition at low temperature for the magnetic ions. The inverse susceptibility data (shown in the inset of Fig. 9a) exhibit only a paramagnetic region within the range 540–690 K. The curve can be fitted with a Curie–Weiss law:

$$\chi = \frac{C}{T - \theta_p},$$

where C is the Curie constant and θ_p the paramagnetic Curie temperature independent susceptibility. The fit gave $C = 1.91 \text{ cm}^3 \text{ K mol}^{-1}$ and $\theta_p = -950 \text{ K}$. The magnetic moment estimated from the Curie–Weiss constant is $\mu_{\text{eff}} = 3.9 \mu_B \text{ f.u.}^{-1}$, in good agreement with the value calculated from the spin-only contribution and chemical analyses, considering one Cr^{3+} H.S. in the $[\text{CrO}_2]$ layers and 0.1 Cr^{6+} to the part substituted to Bi ions (23) ($\mu_{\text{eff}} = 3.9 \mu_B \text{ f.u.}^{-1}$). The strongly negative value of θ_p is indicative of antiferromagnetic interactions; the onset of the magnetic order can be seen in Fig. 9a at 130 K. This synthesized material exhibits a strong insulating behavior at room temperature.

TABLE 5

^{57}Fe Mössbauer Hyperfine Parameters of $\text{Bi}_{0.4}\text{Sr}_{2.5}\text{Fe}_{1.1}\text{O}_5$ Phase at Room Temperature

Site	IS (mm s^{-1})	QS (mm s^{-1})	% ($\pm 5\%$)	Ion charge
A	0.21	0.75	47	+3
B	0.08	0.67	40	+4
C	0.13	0.25	13	+4

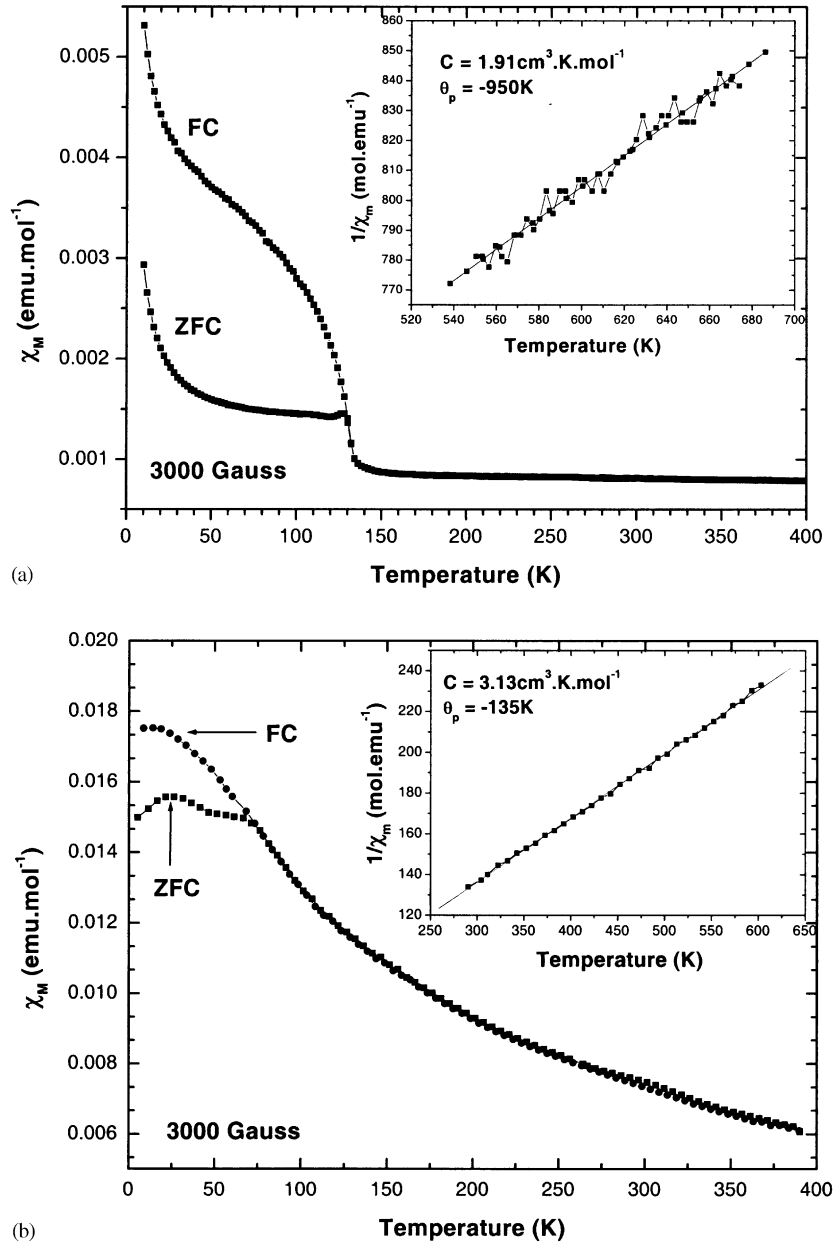


FIG. 9. $\chi_M(T)$ curves obtained from ZFC and FC $M(T)$ curves recorded in 3000 G. Inset: $\chi^{-1}(T)$ curve (symbols are experimental points whereas solid line is the fit).

$Bi_{0.4}Sr_{2.5}Fe_{1.1}O_5$

The magnetic susceptibility measurements were performed in the range 5–600 K (Fig. 9b). The change of slope in the zero-field cooling curve (ZFC) below 70 K indicates the existence of an antiferromagnetic transition with $T_N \approx 70$ K. The hysteresis between ZFC and FC could result from the stronger spin canting induced by the FC process. For $T > 250$ K, the linear part of χ^{-1} (inset of Fig. 9b), fitted with the Curie–Weiss law leads to a negative θ_p values (–135 K), typical of antiferromagnetic interac-

tions and an effective paramagnetic moment μ_{eff} of $5.0 \mu_B \text{ mol}^{-1}$ of product. Considering the ratio 50:50 of Fe^{3+}/Fe^{4+} determined by Mössbauer spectroscopy, XANES and chemical titration, the μ_{eff} value agrees well with a combination of low- and high-spin configurations for Fe^{4+} and Fe^{3+} , respectively. Taking account of these usual electronic configurations, the μ_{eff} value is calculated as $4.9 \mu_B \text{ f.u.}^{-1}$.

In spite of presence of the Fe^{3+}/Fe^{4+} mixed valence, the resistivity of this phase is very high at low temperature, reaching the maximum measurable value with our setup

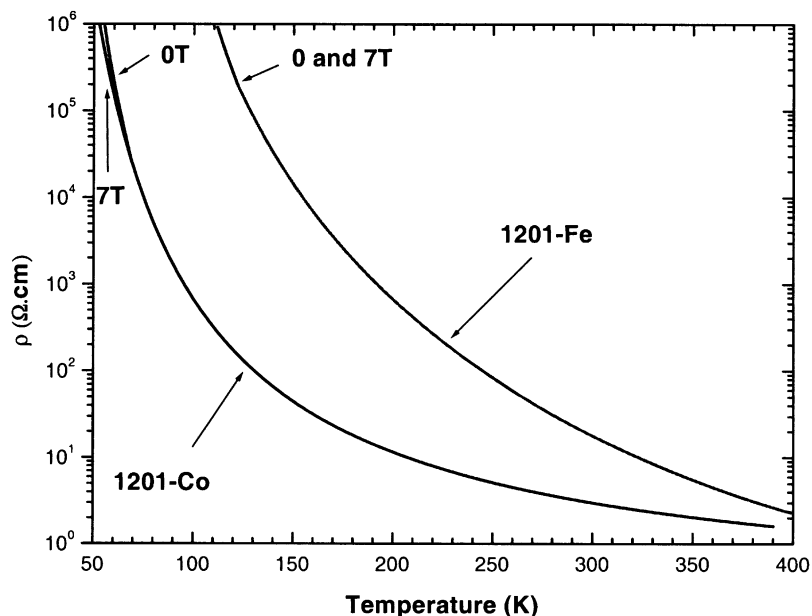


FIG. 10. T dependence of the resistivity registered during cooling in 0 and in 7 T for $\text{Bi}_{0.4}\text{Sr}_{2.5}\text{Fe}_{1.1}\text{O}_5$ and $\text{Bi}_{0.4}\text{Sr}_{2.45}\text{Co}_{1.15}\text{O}_{4.85}$ (9).

($10^7 \Omega \text{cm}$) at 100 K. The dramatic decrease of ρ from $2 \times 10^5 \Omega \text{cm}$ at 120 K to $2.2 \Omega \text{cm}$ at 400 K (Fig. 10) shows the semiconductor-like behavior of this phase with $E_a = 1.2 \text{ eV}$. More importantly, the resistivity of this bismuth ferrite ($\rho_{300 \text{ K}} = 18 \Omega \text{cm}$) is close to that of the Bi–Sr 1201 cobaltite ($\rho_{300 \text{ K}} = 3 \Omega \text{cm}$), i.e., considerably smaller than that of the manganite $\text{Bi}_{0.4}\text{Sr}_{2.6}\text{MnO}_{4.7}$ (8) ($\rho_{300 \text{ K}} = 2.3 \times 10^3 \Omega \text{cm}$) and the chromite ($\rho_{300 \text{ K}} > 10^6 \Omega \text{cm}$). Although the $\rho(T)$ curves, of both Co- and Fe-based 1201 are very similar, it should be emphasized that the former exhibits a negative magnetoresistance, 0–25% in 7 T at 50 K, whereas no MR is detected for the latter as shown in Fig. 10 where the $\rho_{0 \text{ T}}(T)$ and $\rho_{7 \text{ T}}(T)$ curves are given. The existence of small metallic ferromagnetic regions in the cobaltite, which grow under magnetic field application so that ρ decreases, cannot occur in the antiferromagnetic ferrite under study.

CONCLUSION

This work highlights the richness of the Bi–Sr– M –O systems, especially because of the mixed ordered Bi:Sr rocksalt-type layers, and evidences the great flexibility of the 1201-type stacking which accommodates to numerous ($M = \text{Mn}, \text{Co}, \text{Fe}, \text{and Cr}$) transition elements. The existence of continuous $\text{Fe}_{1-y}\text{M}_y$ solid solutions has been demonstrated even if complementary neutron structural studies will be necessary to clarify the oxygen stoichiometry and the nature of the MO_x polyhedra. In this way, numerous combinations between the transition elements

can be clarified for studying the transport properties. This work is actually in progress in order to demonstrate also some possible magnetic interactions between M elements.

REFERENCES

1. C. Michel, M. Hervieu, M. M. Borel, A. Grandin, and F. Deslandes, J. Provost, and B. Raveau, *Z. Phys. B* **68**, 421 (1987).
2. M. Maeda, Y. Tanaka, M. Fukutomi, and T. Asano, *Jpn. J. Appl. Phys.* **L27**, 209 (1988).
3. J. M. Tarascon, W. R. McKinnon, P. Barboux, D. M. Hwang, B. G. Babley, L. H. Greene, G. H. Hull, Y. Lepage, N. Stoffel, and M. Giroud, *Phys. Rev. B* **38**, 8885 (1988).
4. J. M. Tarascon, P. F. Miceli, P. Barboux, D. M. Hwang, G. W. Hull, M. Giroud, and L. H. Greene, *Phys. Rev. B* **39**, 16 (1989).
5. J. M. Tarascon, Y. Le Page, and W. R. McKinnon, *Eur. J. Solid State Inorg. Chem.* **27**, 81–104 (1990).
6. D. Pelloquin, M. Allix, C. Michel, H. Hervieu, and B. Raveau, *Philos. Mag. B* **81**(11), 1669–1685 (2001).
7. D. Pelloquin, A. C. Masset, A. Maignan, M. Hervieu, C. Michel, and B. Raveau, *J. Solid State Chem.* **148**, 108–118 (1999).
8. D. Pelloquin, A. Maignan, M. Hervieu, C. Michel, and B. Raveau, *J. Solid State Chem.* **151**, 210–219 (2000).
9. A. C. Masset, O. Toulemonde, D. Pelloquin, E. Suard, A. Maignan, F. Studer, M. Hervieu, and C. Michel, *Int. J. Inorg. Mat.* **2**, 687–699 (2000).
10. M. Hervieu, C. Michel, N. Nguyen, R. Retoux, and B. Raveau, *Eur. J. Solid State Inorg. Chem.* **25**(4), 375 (1988).
11. M. Hervieu, C. Michel, D. Pelloquin, A. Maignan, and B. Raveau, *J. Solid State Chem.* **132**, 420–431 (1997).
12. Y. Breard, C. Michel, M. Hervieu, and B. Raveau, *J. Mater. Chem.* **10**, 1043–1045 (2000).
13. K. Yamaura, Q. Huang, J.W. Lynn, R.W. Erwin, and J. Cava, *J. Solid. State Chem.* **152**, 374–380 (2000).

14. J. Rodriguez-Carvajal, "Collected Abstract of the Satellite Meeting on Powder Diffraction of the XVth Congress of the International Union of Crystallography, Toulouse, France, p. 127," 1990.
15. C. Martin, D. Bourgault, C. Michel, J. Provost, M. Hervieu, and B. Raveau, *Eur. J. Solid State Inorg. Chem.* **26**, 1 (1955).
16. B. Aurivilius, *Acta. Chem. Scand.* **9**, 1219 (1955).
17. G. Malmros, *Acta. Chem. Scand.* **24**, 384 (1970).
18. K. J. Rao and J. Wong, *J. Chem. Phys.* **81**, 4832 (1984).
19. R. Blake, R. E. Hessevick, T. Zoltai, and L.W. Finger, *Am. Mineral.* **51**, 123–129 (1996).
20. J. P. Hodges, S. Short, J. D. Jorgensen, X. Xiong, B. Dabrowski, S. M. Mini, and C. W. Kimball, *J. Solid State Chem.* **151**, 190–209 (2000).
21. T. Takeda and H. Watanabe, *J. Phys. Soc. Jpn.* **33**, 973 (1972).
22. O. Toulemonde, F. Studer, A. Barnabe, A. Maignan, C. Martin, and B. Raveau, *Eur. Phys. J* **B4**, 159 (1998).
23. S. Malo, C. Michel, D. Pelloquin, M. Hervieu, O. Toulemonde, and B. Raveau, *Physica C* **213**, 304 (1998).
24. N. Natoli, A. Bianconi, L. Incoccia, and S. Stipcich, in "EXAFS and Near Edge Structure," Springer Series in Thermal Physics, Vol. 27. Springer-Verlag, Frascati, Italy, September 13–17, 1983.